JOURNAL OF CATALYSIS 128, 526–536 (1991)

Influence of Metal Particle Size and Support on the Catalytic Properties of Supported Rhodium: $CO-O_2$ and CO–NO Reactions

SE H. OH AND CAROLYN C. EICKEL

Physical Chemistry Department, General Motors Research Laboratories, Warren, Michigan 48090-9055

Received July 17, 1990; revised October 9, 1990

The effects of metal particle size and support material on the kinetics of the $CO-O_2$ and CO–NO reactions over Rh have been investigated. For the $CO-O_2$ reaction in the CO-inhibition regime, both the specific rate and the apparent activation energy were found to be virtually independent of the Rh particle size, but moderately sensitive to the nature of the support material (with the low-temperature oxidation activity decreasing in the order $Rh/\alpha-Al_2O_3 > Rh/SiO_2 > Rh/\theta-Al_2O_3$). The specific rate of the CO–NO reaction increased drastically with increasing Rh particle size; a 45-fold increase in specific rate was observed as the Rh particle size increased from 10 to 676 Å. However, support material had only a small effect on both the activity and selectivity of Rh for the CO–NO reaction.

INTRODUCTION

The reaction of CO with O_2 or NO over supported noble metal catalysts is an important part of the catalytic control of automobile exhaust emissions (*1, 2*). Rhodium is an essential constituent of three-way catalysts and exhibits excellent activity for both CO oxidation and NO reduction. As such, the kinetics and mechanism of the $CO-O_2$ reaction (*3–8*) and the CO–NO reaction (*7–11*) over Rh catalysts have received considerable attention in the literature of the past decade.

Besides their importance in automobile exhaust catalysis, these two reactions provide interesting examples of differing structure sensitivity. Our earlier work conducted in collaboration with Sandia National Laboratories (*7, 8*) has shown that there are close similarities in the kinetics of the $CO-O_2$ reaction over single crystal (Rh(111) and Rh(100)) and supported (Rh/Al_2O_3) catalysts, whereas the CO–NO reaction exhibits drastically different kinetic behavior between these two types of Rh catalysts. Specifically, the kinetics of the CO–NO reaction measured over Rh single crystals were characterized by substantially lower apparent activation energies and higher specific rates than those measured over supported Rh. Thus, the kinetics of the CO–NO reaction, unlike the $CO-O_2$ reaction kinetics, are sensitive to the environment of the rhodium in the catalyst.

This study was undertaken to clarify the origins of the structure sensitivity observed for the CO–NO reaction between supported and unsupported (i.e., single crystal) Rh. Factors that might be involved in such structure sensitivity include effects of (1) crystallographic orientation, (2) support material, and (3) rhodium particle size. A recent kinetic study with Rh(111) and Rh(100) single crystals (*8*) has shown that the kinetics of the CO–NO reaction are moderately sensitive to the crystallographic orientation of the surface; however, the observed difference in specific reaction rates between these two crystal planes was too small to account for the activity difference between single crystal and supported Rh catalysts reported in our earlier study (*7*). In this paper we examine the other two factors that might be responsible for the structure sensitivity: the effects of support materials and rhodium particle size. Investigation of these two factors might provide useful insights into the

0021-9517/91 $3.00

origins of the observed sensitivity of the CO–NO reaction kinetics to the rhodium environment because a Rh single-crystal catalyst represents a special case of large unsupported metal crystallites. Although our principal focus is on the dependency of the CO–NO reaction kinetics on support material and Rh crystallite size, parallel experiments have also been conducted for the $CO-O_2$ reaction for comparison purposes.

These experiments were prompted not only by the question of structure sensitivity described above, but also by the practical implications of support material and metal particle size in the catalytic control of automobile exhaust emissions. Support materials have been reported to have profound effects on the poison resistance, thermal stability, and catalytic activity of Rh-containing automotive catalysts (*12–15*). Also, the growth of noble metal particles has been identified as an important deactivation mode of automotive catalysts during vehicle use (*16, 17*).

EXPERIMENTAL

Catalyst Preparation

Three different supports, all in the form of spherical pellets of ~3-mm diameter, are employed in this study: θ–Al_2O_3 (W. R. Grace, 112 m^2/g), α–Al_2O_3 (5 m^2/g), and SiO_2 (United Catalysts, 131 m^2/g). The α–Al_2O_3 support was obtained by calcining the θ–Al_2O_3 at 1200°C for 2 h. The characteristics of the catalyst samples used in the experiments are listed in Table 1. The catalysts supported on θ–Al_2O_3 and α–Al_2O_3 were prepared by the standard incipient wetness procedure with aqueous solutions of $RhCl_3 \cdot 3H_2O$. Following impregnation the catalysts were dried in air overnight at room temperature and then calcined in flowing air at 500°C for 4 h. The Rh/SiO_2 catalyst was prepared by incipient wetness impregnation with a basic (pH ~ 12) solution of $[Rh(NH_3)_6]Cl_3$ dissolved in NH_4OH, followed by air-drying overnight at 120°C, subsequent reduction in 5% H_2 at 300°C for 1 h, and then calcination at 500°C for 4 h.

TABLE 1

Characteristics of Catalyst Samples Used

Sample code	Support	BET area (m^2/g)	Rh loading (wt%)	State	Rh dispersion (%)
A	θ–Al_2O_3	112	0.03	Fresh	100[a]
B	SiO_2	131	0.03	Fresh	100[a]
C	α–Al_2O_3	5	0.03	Fresh	100[a]
D	α–Al_2O_3	5	0.5	Fresh	26.4
E	α–Al_2O_3	5	3	Fresh	9.5
F	α–Al_2O_3	5	3	Sintered[b]	4.0
G	α–Al_2O_3	5	3	Sintered[c]	1.7

[a] Estimated.
[b] 800°C, air, 3 h.
[c] 1000°C, air, 3 h.

Electron microprobe measurements show that such procedures resulted in a shallow (<100 μm) Rh band at the periphery of the θ–Al_2O_3 and SiO_2 beads. The Rh tended to penetrate deeper into the low-surface-area α–Al_2O_3 support, approaching uniform Rh distribution throughout the beads at high Rh loadings (samples D through G in Table 1). These α–Al_2O_3-supported catalyst beads were cleaved in four and the resulting quarter pellets were used for rate measurements to minimize interference from intrapellet diffusion resistances.

For the catalysts prepared for the study of support effects (samples A through C), the Rh loading was fixed at 0.03 wt%. Such a low Rh loading was chosen to obtain highly dispersed catalyst samples, in which most of the Rh atoms are in close contact with the support and thus metal-support interactions are likely to manifest themselves. The catalysts used to study Rh particle size effects (samples C through G) were all prepared on α–Al_2O_3 (generally known as a noninteracting support) in order to minimize support effects. Samples of varying metal particle sizes were obtained either by changing the Rh loading (samples C, D, and E) or by thermal treatments in air (samples F and G).

H_2 Chemisorption

The apparent Rh dispersions listed in Table 1 were measured by static H_2 chemisorption in a Micromeritics ChemiSorb 2800 au-

tomated chemisorption instrument. A sample size of ~2 g was used with the following sequence of pretreatments: (1) 5% O_2 at 450°C for 1 h, (2) 5% H_2 at 250°C for 1 h, (3) evacuation at 250°C for 2 h, and (4) cooling to 35°C under vacuum. The chemisorption measurements were carried out at 35°C; the total H_2 uptake was determined first and then the sample was evacuated and redosed with H_2 to measure the reversible H_2 uptake. The irreversible H_2 uptake, obtained by subtracting the reversible uptake from the total uptake, was used to calculate the Rh dispersion assuming 1 : 1 chemisorption stoichiometry between surface Rh atoms and adsorbed hydrogen atoms.

In view of their low (0.03 wt%) Rh loading, the Rh in samples A, B, and C was assumed to be 100% dispersed. This assumption seems reasonable in view of the results of chemisorption measurements for Rh/γ–Al_2O_3 (*18*) and for Rh/SiO_2 (*11*). Although the Rh dispersion for the 3 wt% Rh/α–Al_2O_3 catalyst decreased substantially after the sintering treatments, the H_2 uptakes of aged samples F and G were still sufficiently high (>2 μmol/g) for reliable dispersion measurements.

Transmission Electron Microscopy

The Rh particle size distributions of catalyst samples E, F, and G were determined using a Philips 430 high-voltage electron microscope operating at 300 keV. Samples for TEM analysis were prepared by crushing and grinding the catalyst beads in a mortar. The resulting fine powder was ultrasonically dispersed in methanol and a drop or two of the suspension was deposited on carbon-coated copper grids. After drying at room temperature, the copper grids were inserted in the TEM without further treatment. For each sample, the diameters of several hundred particles were measured from the electron micrographs to obtain the Rh particle size distribution.

Rate Measurements

The experimental apparatus and procedures used for rate measurements are identical to those described previously (*6*). Steady-state reaction rates were measured in laboratory CO–NO or CO–O_2 feedstreams (in a N_2 background) using a stainless-steel internal-recycle mixed-flow reactor (*19*) equipped with continuous gas analyzers (nondispersive IR for CO and CO_2, chemiluminescence detection for NO, and polarographic detection for O_2). The internal surfaces of the reactor were coated with a thin layer of aluminum oxide to minimize the blank activity, and gas-phase mixing within the reactor is provided by a magnetically driven impeller placed under the stationary catalyst basket. All the experiments reported here were done at atmospheric total pressure using an impeller speed of 1500 rpm and a total feedstream flow rate of 5 l/min (STP) through 2 to 4 g of catalyst. These experimental conditions provided good gas-phase mixing within the reactor, thus allowing the reactor to be characterized as a CSTR. Prior to each kinetic experiment the catalyst sample was treated in flowing 2 vol% O_2 at 450°C for 30 min and then reduced in flowing 5 vol% H_2 at 250°C for 15 min. Earlier kinetic (*11*) and temperature-programmed reduction (*20*) studies of supported Rh catalysts, as well as our chemisorption results presented later in this paper, indicate that the latter reducing treatment is sufficient to reduce all the surface Rh oxides to Rh metal even after high-temperature oxidation of the samples.

RESULTS AND DISCUSSION

Rh Particle Size: TEM vs Chemisorption

Figure 1 shows particle size distributions determined from TEM examinations of the 3 wt% Rh/α–Al_2O_3 catalyst before and after sintering treatments. In the fresh sample (prereduced at 250°C; see Fig. 1a), nearly all rhodium particles were between 20 and 80 Å in diameter. Figure 1b shows the results for the 3 wt% Rh/α–Al_2O_3 catalyst which was sintered in air at 800°C for 3 h. Although a broad particle size distribution is observed here, it is evident that the 800°C sintering treatment caused the population of large particles to increase at the expense of

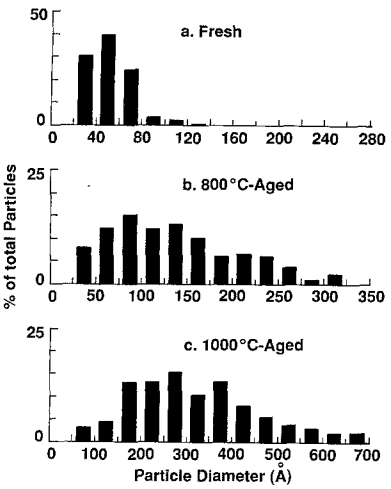

FIG. 1. TEM-derived metal particle size distributions for the 3 wt% Rh/α–Al_2O_3 catalyst before and after sintering in air.

small particles. An increase in the sintering temperature from 800 to 1000°C resulted in further growth of particles, with the majority of the particles lying in the broad size range of 150 to 500 Å in diameter (see Fig. 1c). It should be noted that the particle size distribution data shown in Figs. 1b and 1c were those of Rh oxide (not Rh metal) because they were measured after the sintering treatments in air without subsequent reduction. Although not directly examined in this study, the size distributions of the Rh metal particles present in the reduced, sintered catalysts would be expected to be similar to those shown in Figs. 1b and 1c; Wong and McCabe (*21*) have recently shown that a mild (200°C) reduction treatment of high-temperature-oxidized Rh/SiO_2 catalysts did not significantly change the particle size distribution.

Table 2 lists three statistical averages calculated from the TEM-derived particle size distribution data of Fig. 1: number-averaged (d_n), surface-averaged (d_s), and volume-averaged (d_v) particle sizes. Also shown in Table 2 are the average particle diameters (d_c) calculated from H_2 chemisorption results assuming spherical metal particles (*22*). Comparisons of d_s and d_c for all three samples indicate that the chemisorption measurements generally overestimate the metal particle size by 20 to 80%.

The reasons for these discrepancies between the chemisorption-derived and TEM-observed particle sizes are not clear. One possible explanation is that H_2 is known to adsorb dissociatively on Rh (*23*) and thus unlikely to adsorb irreversibly on the isolated Rh atoms (*24*), which might be present in our catalysts in significant amounts. In this case, H/Rh ratios characteristic of the size of the 3-dimensional Rh particles (i.e., those observable by TEM) should be based on the amount of Rh in the particulate phase and not based on the total amount of Rh. Therefore, the values of H/Rh listed in Table 1 (which were calculated based on the total amount of Rh) may not be directly indicative of Rh particle size, and tend to overestimate the average size of the 3-dimensional Rh particles as observed here.

Another possibility for the discrepancy between the TEM and chemisorption results might be that a significant fraction of the Rh surface is inaccesible to H_2 chemisorption as a result of either site blocking by surface impurities (e.g., chloride ion derived from the metal precursor; Refs. (*25*) and (*26*)) or the decoration of the Rh particles by partially reduced support moieties (a phenomenon commonly referred to as SMSI). We did not pursue the possibility of impurity-induced suppression of chemisorption. However, the SMSI argument can be ruled out on the basis of the results of H_2 chemisorption measurements shown in Table 3. As expected for the "noninteracting" sup-

TABLE 2

Average Particle Sizes for 3 wt% Rh/α–Al_2O_3 Catalyst

Sample	TEM			Chemisorption
	d_n (Å)	d_s (Å)	d_v (Å)	d_c (Å)
Fresh	52	67	74	121
800°C Aged	145	240	283	288
1000°C Aged	316	434	479	676

TABLE 3

H_2 Uptake of 0.5 wt% $Rh/\alpha-Al_2O_3$ as a Function of Reduction Temperature

Reduction temperature[a] (°C)	H_2 uptake (μmol/g)
250	5.89
450	6.24
750	4.56

[a] Preceded by 5% O_2 treatment at 450°C in all cases.

port $\alpha-Al_2O_3$, no drastic suppression of H_2 uptake was observed even after high-temperature reduction, which is known to promote an SMSI state (*27*). The difference between H_2 uptakes measured after the 250 and 450°C reduction treatments is small (~6%), and the moderate decrease in H_2 uptake after 750°C reduction is presumably related to the usual sintering of the Rh particles, rather than SMSI.

In this work H_2 chemisorption is taken as a measure of the surface Rh atoms which actually participate in the catalytic reactions of interest here. Besides its reasonably well-established adsorption stoichiometry on Rh, H_2 chemisorption may have the added advantage of "counting" primarily contiguous Rh surface atoms (*23, 24*) which have been shown to be much more active catalytically than isolated Rh sites (*28, 29*). The validity of using H_2 chemisorption to determine the active metal surface area is further demonstrated by the observation of good correlation between catalytic activity and chemisorption for CO oxidation over a wide range of Rh particle sizes. This aspect is discussed in the next section.

Influence of Rh Particle Size

A. *$CO-O_2$ reaction.* Table 4 shows the turnover numbers and the apparent activation energies for the CO oxidation, measured at 1 vol% CO and 1 vol% O_2, as a function of Rh particle size. The turnover numbers (i.e., the number of CO_2 molecules produced per surface Rh atom per second) were obtained by normalizing the measured reaction rates to the total number of surface Rh atoms determined from H_2 chemisorption measurements. It can be seen from Table 4 that the CO oxidation over Rh is characterized by relatively constant turnover numbers (0.0401 ± 0.0053 at 150°C and 0.0600 ± 0.0074 at 155°C) over a wide range of Rh particle sizes, the relative standard deviations being ~13%. This observation is consistent with the conclusion of earlier work (*7, 8, 30, 31*) that both the adsorption and oxidation of CO on Rh are structure insensitive. The apparent activation energies for the CO oxidation reaction listed in Table 4 are in good agreement with values reported previously (*7, 8*), and are similar to the activation energy for CO desorption from CO-saturated Rh surfaces (*7, 31, 32*). For all five catalyst samples studied, the rate of the $CO-O_2$ reaction was found to be directly proportional to O_2 partial pressure and inversely proportional to CO partial pressure.

All the kinetic behavior described above can be interpreted on the basis of a reaction mechanism in which the catalyst surface is predominantly covered with adsorbed CO under reaction conditions and the reaction rate is limited by oxygen adsorption onto vacant Rh sites created primarily by CO desorption (*4, 7*). Also, the constancy of the turnover number, apparent activation energy, and reaction orders observed here

TABLE 4

Turnover Number and Activation Energy for $CO-O_2$ Reaction as a Function of Rh Particle Size

Sample code	Dispersion (particle size)	Turnover number (s^{-1})		Activation energy (kcal/mol)
		150°C	155°C	
C	100% (<10 Å)	—	0.0648[a]	24
D	26.4% (44 Å)	0.0387	0.0565	28
E	9.5% (121 Å)	0.0435	0.0650	29
F	4.0% (288 Å)	0.0331	0.0485	31
G	1.7% (676 Å)	0.0449	0.0654	28

[a] Calculated assuming 100% Rh dispersion.

TABLE 5

Turnover Number and Activation Energy for CO–NO Reaction as a Function of Rh Particle Size

Sample code	Dispersion (particle size)	Turnover number (s^{-1})		Activation energy (kcal/mol)
		215°C	230°C	
C	100% (<10 Å)	—	0.0166[a]	30, 39
D	26.4% (44 Å)	0.0196	0.0535	32, 37
E	9.5% (121 Å)	0.0320	0.0790	27, 36
F	4.0% (288 Å)	0.123	0.386	32
G	1.7% (676 Å)	0.253	0.741	33

[a] Calculated assuming 100% Rh dispersion.

over the wide Rh particle size range suggests that the above-mentioned reaction mechanism for the CO oxidation remains unchanged upon Rh particle size variation. It is also interesting to note that the turnover numbers presented in Table 4, when extrapolated to higher temperatures assuming an apparent activation energy of 29 kcal/mol, correlate very well with the rate data reported by Oh *et al.* (*7*) for single-crystal Rh(111) and alumina-supported Rh catalysts. This suggests the possibility that CO oxidation rate measurements can be used to determine the total number of surface Rh atoms that actually participate in the catalytic reaction.

B. *CO–NO reaction.* The results of kinetic experiments for the CO–NO reaction are summarized in Table 5, where the turnover numbers and the apparent activation energies are shown as a function of Rh particle size. The data were generated during temperature run-up experiments in a reactant gas mixture containing 1 vol% CO and 0.5 vol% NO. It is evident in Table 5 that in contrast to the CO–O_2 reaction kinetics just discussed, the turnover number for the CO–NO reaction increases substantially with increasing Rh particle size. At 230°C, for example, a 45-fold increase in the turnover number was observed as the Rh particle size increased from <10 to 676 Å. The rate data obtained at 215°C also exhibit the same trend; the turnover number increased by a factor of 13 with an increase in particle size from 44 to 676 Å. (The rate over sample C at 215°C was too low to measure reliably.)

Arrhenius plots of the rate data for the CO–NO reaction over samples C, D, and E revealed a discontinuity and therefore two distinct apparent activation energies are reported in Table 5: the first one for the low-temperature regime and the second for the higher-temperature regime. Such an increase in activation energy with temperature has been reported previously for supported Rh (*10, 33*), and generally reflects a shift in the rate-controlling step to an alternate or parallel path (*34*). A kinetic analysis of the CO–NO reaction by Oh (*33*) indicates that the rate-controlling step may shift from the low-temperature N_2/N_2O formation path (involving reactions between NO_a and N_a) to the high-temperature N_2 formation path (involving recombination of N_a) as the catalyst temperature is increased. For the cases of large Rh particle sizes (samples F and G), however, Arrhenius plots of the reaction rates are well represented by single apparent activation energies, similar to those previously reported for Rh(111) single crystals (*7, 8*), over the temperature range of our kinetic experiments, as listed in Table 5. This observation can be explained on the basis of the NO TPD results of Altman and Gorte (*35*), which showed that for large Rh particles most N_2 desorbs in a low-temperature peak centered near 190°C (attributed to the $NO_a + N_a$ reaction), with a relatively small amount of N_2 desorbing above 280°C. In this case, the low-temperature path (due to its higher peak intensity and lower activation energy) would proceed at a rate much faster than that of the high-temperature path and thus dominate the kinetics of the CO–NO reaction, allowing the temperature dependence of the rate data to be characterized by a single activation energy. The same TPD study has also shown that the relative intensity of the low- and high-temperature peaks changes dramatically with Rh particle size; that is, as the particle size is decreased,

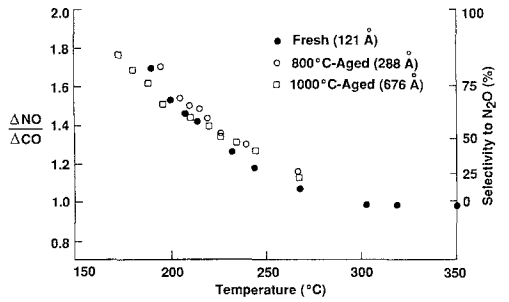

FIG. 2. Selectivity to N_2O as a function of temperature for the CO–NO reaction over fresh and aged 3 wt% Rh/α–Al_2O_3 in a feedstream containing 1 vol% CO and 0.1 vol% NO.

the high-temperature N_2 desorption peak (attributed to N_a recombination) grows at the expense of the low-temperature N_2 desorption feature. As proposed previously (*35*), such changes in the N_2 desorption features with particle size are likely to be responsible for the structure sensitivity of the CO–NO reaction kinetics observed in Table 5. The slow removal of N_2 from the surface of small Rh particles at low temperatures resulting from the suppression of the NO_a + N_a reaction step can explain the observation that the turnover numbers for small particles are substantially lower than those for large ones.

It is interesting to note that despite the wide variation of the NO reduction activity with Rh particle size, the product distribution between N_2O and N_2 for the CO–NO reaction appears to be little affected by the size of Rh particles. It has been shown (*33*) that the selectivity to N_2O is directly related to the CO–NO reaction stoichiometry characterized by the ratio between ΔCO and ΔNO. (The symbol Δ here refers to the amounts of the individual reactants consumed during the reaction.) Figure 2 shows plots of $\Delta NO/\Delta CO$ versus temperature measured for fresh and aged samples of the 3 wt% Rh/α–Al_2O_3 catalyst as a convenient way to display the selectivity for forming N_2O versus N_2 (see the *y*-axis on the right). In accord with results previously reported for supported Rh (*10, 33, 36*), the product selectivity for all three samples of the Rh/α–Al_2O_3 catalyst is dominated by N_2O formation at low temperatures and by N_2 formation at high temperatures. Also, the data points for the three samples in Fig. 2 are clustered reasonably closely, indicating that the selectivity of Rh/α–Al_2O_3 for the CO–NO reaction, unlike its activity, is insensitive to changes in Rh particle size.

Recall that the turnover numbers reported in Tables 4 and 5 represent the reaction rates per surface Rh atom which chemisorbs H. From a practical point of view, it would be interesting to examine how the overall rate (e.g., rate per gram Rh) changes with Rh particle size. Figure 3 shows the overall rates, calculated from Tables 4 and 5, as a function of Rh dispersion for both the CO–NO (at 230°C) and CO–O_2 (at 155°C) reactions. As might be expected from the structure insensitivity of the CO–O_2 reaction, its overall rate is directly proportional to the Rh dispersion; the reaction rates per gram Rh traverse nearly 2 orders of magnitude over the Rh dispersion range of 1.7 to 100% (or over the Rh particle size range of <10 to 676 Å). The overall rate of the CO–NO reaction, on the other hand, exhib-

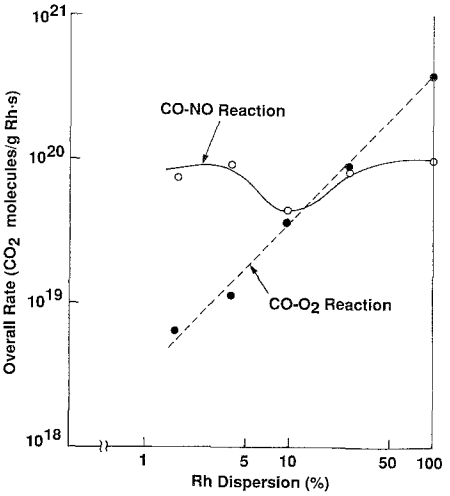

FIG. 3. Overall rates for the CO–O_2 and CO–NO reactions as a function of Rh dispersion.

its a relatively small variation (twofold as opposed to 2 orders of magnitude) over the same particle size range. Of course, this small variation in overall rate for the CO–NO reaction is due to the fact that the loss of active metal surface area resulting from Rh particle growth is largely offset by the attendant increase in turnover number. The results of Fig. 3 provide an explanation for the previous observations that thermal aging of Rh/Al_2O_3 catalysts improves the selectivity for NO conversion in $CO–NO–O_2$ mixtures (*37–39*).

Influence of Support

Having observed the dramatic Rh particle size effect on the turnover number for the NO reduction, it is interesting to examine how the rate of the CO–NO reaction over supported Rh depends on the support material used. We made only cursory examinations of support effects using low-loaded (0.03 wt%) Rh catalysts supported on SiO_2, $\alpha–Al_2O_3$, and $\theta–Al_2O_3$. At such a low Rh loading, it is expected that most of the Rh atoms would be in direct contact with the support and thus metal-support interactions, if any, would likely manifest themselves in changes in the catalytic properties. Figure 4 presents Arrhenius plots of the CO–NO reaction rates measured over Rh/SiO_2, $Rh/\alpha–Al_2O_3$, and $Rh/\theta–Al_2O_3$ at CO and NO concentrations of 1 and 0.5 vol%, respectively. The turnover numbers shown in Fig. 4 were calculated assuming that all the Rh atoms in these low-loaded catalysts participate in the catalytic reactions. Over the temperature range investigated (240–290°C), the NO reduction activity decreases in the order $Rh/\alpha–Al_2O_3 > Rh/SiO_2 > Rh/\theta–Al_2O_3$, but the support effect is generally seen to be relatively small (i.e., less than twofold variation in activity). Also, the apparent activation energy for Rh/SiO_2 (43 and 49 kcal/mol at low and high temperatures, respectively) is substantially higher than that for $Rh/\alpha–Al_2O_3$ (30 and 39 kcal/mol) or that for $Rh/\theta–Al_2O_3$ (32 and 38 kcal/mol). The relative activity and apparent activation energy of Rh/SiO_2 and $Rh/\theta–Al_2O_3$ observed here are in accord with the results of Pande and Bell (*40*).

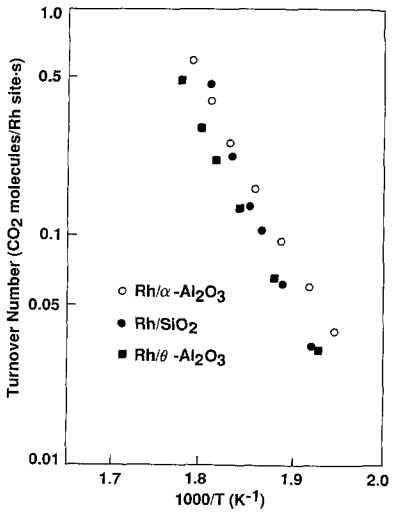

FIG. 4. Arrhenius plots of the CO–NO reaction rates measured over $Rh/\alpha–Al_2O_3$, Rh/SiO_2, and $Rh/\theta–Al_2O_3$ at 1 vol% CO and 0.5 vol% NO.

The weak dependence of the CO–NO reaction kinetics on support material is also reflected in measurements of the product selectivity, as shown in Fig. 5 for a feedstream containing 1 vol% CO and 0.1 vol% NO. Although there is some scatter in the low-temperature data (due primarily to low NO conversions), it is apparent that support material has only a minor effect on the selectivity of Rh for NO reduction by CO. In agreement with earlier studies (*10, 33, 36, 40*), N_2O is the major nitrogen-containing reaction product at low temperatures while N_2 formation is favored at high temperatures, for all of the three supports examined.

It is interesting to note that the support has a somewhat stronger influence on the $CO–O_2$ reaction kinetics than it does on the CO–NO reaction kinetics. The rates of the $CO–O_2$ reaction measured over Rh/SiO_2, $Rh/\alpha–Al_2O_3$, and $Rh/\theta–Al_2O_3$ at 1 vol% CO and 1 vol% O_2 are compared in Arrhenius plots shown in Fig. 6. The data exhibit a moderate dependence of the CO oxidation activity on support, and the activity ranking

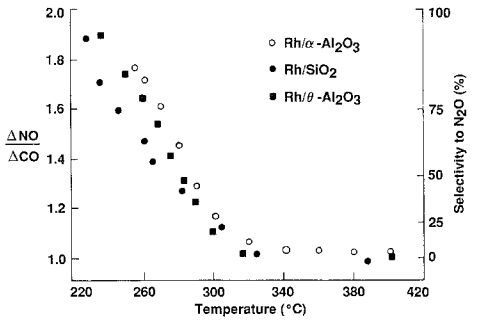

FIG. 5. Selectivity to N_2O as a function of temperature for the CO–NO reaction over Rh/α–Al_2O_3, Rh/SiO_2, and Rh/θ–Al_2O_3 in a feedstream containing 1 vol% CO and 0.1 vol% NO.

for low temperatures (<190°C) is given by Rh/α–Al_2O_3 > Rh/SiO_2 > Rh/θ–Al_2O_3. The apparent activation energy obtained from Fig. 6 decreases in the order Rh/SiO_2 (36 kcal/mol) > Rh/θ–Al_2O_3 (31 kcal/mol) > Rh/α–Al_2O_3 (24 kcal/mol). For all three catalysts, the rate of CO oxidation was found to be inhibited by CO (approximately negative first-order dependence) and enhanced by O_2 (approximately first-order dependence).

The underlying reasons for the observed variation in the CO oxidation activity of Rh with support are uncertain. The same CO and O_2 partial pressure dependences of the rate for Rh/α–Al_2O_3, Rh/SiO_2, and Rh/θ–Al_2O_3 suggest that the same reaction mechanism prevails for all of these catalysts. That is, regardless of the nature of the support, the Rh surface may be predominantly covered with adsorbed CO under reaction conditions, with the CO oxidation rate being limited by the adsorption of oxygen onto vacant Rh sites created primarily by CO desorption. In this case, the apparent activation energy for the CO oxidation would be directly related to the adsorption strength of CO on the Rh surface (*4, 7*). This suggests that the strength of the metal-carbon bond of the adsorbed CO molecule is significantly affected by the nature of the support and decreases in the order Rh/SiO_2 > Rh/θ–Al_2O_3 > Rh/α–Al_2O_3. Such a variation in metal-CO bond energy with support is likely to arise from an electronic interaction between the metal and support. For example, Mori *et al.* (*41*) presented IR evidence that the C–O bond on Rh/SiO_2 is stronger than that on Rh supported on high-surface-area Al_2O_3 or TiO_2. The same authors interpreted their observation on the basis of a difference in the electron density of the metal dispersed on the various oxide supports. It is reasonable to assume that similar electronic effects would also lead to support-induced changes in the metal-CO bond energy (*42, 43*), as suggested by the results of our kinetic measurements.

In addition to giving rise to the electronic interaction mentioned above, the support can also exert a considerable influence on the relative amounts of contiguous Rh atoms and isolated Rh sites on the catalyst surface, as demonstrated by a previous IR study of CO adsorption on Rh catalysts (*44*). In general, both of these support effects are expected to be most pronounced for highly dispersed, low-loaded catalysts such as samples A through C. A quantitative understanding of the metal-support electronic interaction, and of the distribution and reactivity of the various types of Rh sites, would

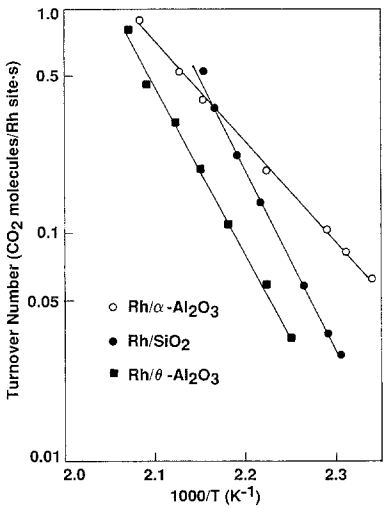

FIG. 6. Arrhenius plots of the CO–O_2 reaction rates measured over Rh/α–Al_2O_3, Rh/SiO_2, and Rh/θ–Al_2O_3 at 1 vol% CO and 1 vol% O_2.

be required in order to fully explain the observed dependence of the CO–O_2 and CO–NO reaction kinetics on support material. These aspects of the behavior of highly dispersed supported Rh catalysts are not yet well understood and await further study.

CONCLUSIONS

Our laboratory reactor experiments have shown that both the turnover number and the apparent activation energy for the CO–O_2 reaction over Rh in the CO-inhibition regime are virtually independent of the metal particle size (when supported on α–Al_2O_3), but are moderately sensitive to the nature of the support material. The apparent activation energy for CO oxidation was found to decrease in the order $Rh/SiO_2 > Rh/\theta$–$Al_2O_3 > Rh/\alpha$–Al_2O_3, and the activity ranking for low temperatures (<190°C) is given by Rh/α–$Al_2O_3 > Rh/SiO_2 > Rh/\theta$–$Al_2O_3$. For the CO–NO reaction, on the other hand, the turnover number increases drastically with increasing Rh particle size (45-fold increase in specific rate as the particle size increased from 10 to 676 Å). This structure sensitivity of the CO–NO reaction correlates with the suppression of the low-temperature N_2 desorption feature ($NO_a + N_a \rightarrow N_2 + O_a$) observed for small Rh particles in a recent TPD study (*35*). It was also observed that support material had only a small effect on both the activity and selectivity of Rh for the CO–NO reaction.

ACKNOWLEDGMENTS

The author thanks M. J. D'Aniello, Jr. (chemisorption data) and S. Kim (TEM micrographs) of the General Motors Research Laboratories.

REFERENCES

1. Taylor, K. C., *in* "Catalysis: Science and Technology" (J. R. Anderson and M. Boudart, Eds.), Vol. 5, p. 119. Springer-Verlag, Berlin, 1984.
2. Kummer, J. T., *Prog. Energy Combust. Sci.* **6,** 177 (1980).
3. Cant, N. W., Hicks, P. C., and Lennon, B. S., *J. Catal.* **54,** 372 (1978).
4. Engel, T., and Ertl, G., "Advances in Catalysis" (D. D. Eley, H. Pines, and P. B. Weisz, Eds.), Vol. 28, p. 1. Academic Press, New York, 1979.
5. Campbell, C. T., Shi, S.-K., and White, J. M., *Appl. Surf. Sci.* **2,** 382 (1979).
6. Oh, S. H., and Eickel, C. C., *J. Catal.* **112,** 543 (1988).
7. Oh, S. H., Fisher, G. B., Carpenter, J. E., and Goodman, D. W., *J. Catal.* **100,** 360 (1986).
8. Peden, C. H. F., Goodman, D. W., Blair, D. S., Berlowitz, P. J., Fisher, G. B., and Oh, S. H., *J. Phys. Chem.* **92,** 1563 (1988).
9. Root, T. W., Schmidt, L. D., and Fisher, G. B., *Surf. Sci.* **150,** 173 (1985).
10. Hecker, W. C., and Bell, A. T., *J. Catal.* **84,** 200 (1983).
11. Hecker, W. C., and Breneman, R. B., *in* "Studies in Surface Science and Catalysis" (A. Crucq and A. Frennet, Eds.), Vol. 30, p. 257. Elsevier, Amsterdam, 1987.
12. Kim, G., and Maselli, J. M., SAE Paper No. 770368.
13. Yao, H. C., Stepien, H. K., and Gandhi, H. S., *J. Catal.* 61, 547 (1980).
14. Stepien, H. K., Williamson, W. B., and Gandhi, H. S., SAE Paper No. 800843.
15. Hammerle, R. H., and Wu, C. H., SAE Paper No. 840549.
16. Powell, B. R., and Chen, Y.-L., *Appl. Catal.* **53,** 233 (1989).
17. Kim, S., and D'Aniello, M. J., Jr., *Appl. Catal.* **56,** 23 (1989).
18. Taylor, K. C., and Schlatter, J. C., *J. Catal.* **63,** 53 (1980).
19. Berty, J. M., *Chem. Eng. Prog.* **70,** 78 (1974).
20. Wong, C., and McCabe, R. W., *J. Catal.* **119,** 47 (1989).
21. Wong, C., and McCabe, R. W., *J. Catal.* **107,** 535 (1987).
22. Anderson, J. R., "Structure of Metallic Catalysts." Academic Press, New York, 1975.
23. Cavanagh, R. R., and Yates, J. T., Jr., *J. Catal.* **68,** 22 (1981).
24. Beck, D. D., and Carr, C. J., *J. Phys. Chem.*, in press.
25. Ott, G. L., Delgass, W. N., Winograd, N., and Baitinger, W. E., *J. Catal.* **56,** 174 (1979).
26. Koopman, P. G. J., Kieboom, A. P. G., and van Bekkum, H., *J. Catal.* **69,** 172 (1981).
27. Tauster, S. J., Fung, S. C., and Garten, R. L., *J. Am. Chem. Soc.* **100,** 170 (1978).
28. Cavanagh, R. R., and Yates, J. T., Jr., *J. Chem. Phys.* **74,** 4150 (1981).
29. Dictor, R. A., and Roberts, S., *J. Phys. Chem.* **93,** 2526 (1989).
30. Altman, E. I., and Gorte, R. J., *Surf. Sci.* **195,** 392 (1988).
31. Belton, D. N., and Schmieg, S. J., *Surf. Sci.* **202,** 238 (1988).
32. Thiel, P. A., Williams, E. D., Yates, J. T., Jr., and Weinberg, W. H., *Surf. Sci.* **84,** 54 (1979).

33. Oh, S. H., *J. Catal.* **124,** 477 (1990).
34. Levenspiel, O., "Chemical Reaction Engineering," 2nd ed., p. 32. Wiley, New York, 1972.
35. Altman, E. I., and Gorte, R. J., *J. Catal.* **113,** 185 (1988).
36. Cho, B. K., Shanks, B. H., and Bailey, J. E., *J. Catal.* **115,** 486 (1989).
37. Schlatter, J. C., and Taylor, K. C., *J. Catal.* **49,** 42 (1977).
38. Lester, G. R., Joy, G. C., and Brennan, J. F., SAE Paper No. 780202.
39. Schlatter, J. C., Taylor, K. C., and Sinkevitch, R. M.,"The Behavior of Supported Rhodium in Catalyzing CO and NO Reactions," presented at Adv. in Catal. Chem. Symp., Snowbird, UT, October 1979.
40. Pande, N. K., and Bell, A. T., *J. Catal.* **98,** 7 (1986).
41. Mori, Y., Mori, T., Miyamoto, A., Takahashi, N., Hattori, T., and Murakami, Y., *J. Phys. Chem.* **93,** 2039 (1989).
42. Sarkany, J., and Gonzalez, R. D., *Appl. Catal.* **5,** 85 (1983).
43. Akubuiro, E. C., Verykios, X. E., and Lesnick, L., *Appl. Catal.* **14,** 215 (1985).
44. Woley, S. D., Rice, C. A., Mattson, G. A., Curtis, C. W., Guin, J. A., and Tarrer, A. R., *J. Phys. Chem.* **86,** 2714 (1982).